Supporting Information for

Interfacial Junctions Control Electrolyte Transport Through Charge-Patterned Membranes

*Feng Gao, Aaron Hunter, Siyi Qu, John R. Hoffman, Peng Gao, William A. Phillip**

Department of Chemical and Biomolecular Engineering, University of Notre Dame, Notre Dame, Indiana 46556, United States

* To whom correspondence should be addressed: wphillip@nd.edu

Detailed Experimental Procedure and Calculations

1. Copolymer Synthesis

All chemicals were purchased from Sigma-Aldrich unless noted otherwise. The poly[acrylonitrile-*co*-oligo(ethylene glycol) methyl ether methacrylate-*co*-(3-azido-2-hydroxypropyl methacrylate)] [P(AN-OEGMA-AHPMA)] copolymer was generated by first synthesizing a poly[acrylonitrile-*co*-oligo(ethylene glycol) methyl ether methacrylate-*co*-glycidyl methacrylate] [P(AN-OEGMA-GMA)] copolymer using a free radical polymerization mechanism.[1] After purifying the P(AN-OEGMA-GMA) copolymer by precipitating it in isopropyl alcohol, it was dissolved in dimethyl sulfoxide (DMSO) along with sodium azide (NaN_3), and ammonium chloride (NH_4Cl). The P(AN-OEGMA-GMA) was dissolved at a concentration of 15% (by weight); NaN_3 and NH_4Cl were added such that the molar ratio of GMA:NaN_3:NH_4Cl was controlled at a value of 1:5:7. This solution was placed in an oil bath at 40 °C for 72 hours. The ring opening of the oxirane group of the GMA repeat units by azide generated the P(AN-OEGMA-AHPMA) copolymer.[2] The P(AN-OEGMA-AHPMA) copolymer was precipitated three times in isopropyl alcohol, dried in a vacuum oven, and stored until further use. The chemical structure and composition of the copolymers were confirmed using ^1H nuclear magnetic resonance (NMR) spectroscopy (Bruker Advance III HD400); deuterated dimethyl sulfoxide was used as the solvent. The molar mass of the copolymer was determined using a gel permeation chromatography (GPC) system that included a Waters 515 HPLC pump, a Waters 2414 refractive index detector, three Polymer Standards Services (PSS) columns (GRAM, 104,103, and 102 Å). Dimethylformamide (DMF) at 55 °C was used as the eluent, volumetric flow rate = 1.00 mL min^{-1}. Linear poly(methyl methacrylate) (PMMA) standards (Polymer Standards Service-USA, Inc.,

Amherst, MA) with molar masses ranging from 730 g mol^{-1} to 1,010,000 g mol^{-1} were used for calibration.

2. Membrane Casting by Non-Solvent Induced Phase Separation

The P(AN-OEGMA-AHPMA) parent membranes were prepared using a non-solvent-induced phase separation (NIPS) method. A 20% (by weight) solution of P(AN-OEGMA-AHPMA) in DMSO was prepared, filtered through a 1 μm syringe filter, and stirred slowly overnight to facilitate the release of dissolved gases prior to membrane casting. A small volume of the casting solution was pipetted onto a polyacrylonitrile (PAN) ultrafiltration membrane (PX, PAN 400kDa, Synder Filtration), which was taped onto a glass plate. A doctor blade adjusted to a gate height of 38 μm was used to draw the polymer solution into a uniform thin film. Solvent was allowed to evaporate from the film for 5 min before plunging it into an isopropyl alcohol (nonsolvent) bath. The membrane was kept in the nonsolvent bath overnight and then transferred and stored in deionized (DI) water. The PAN support membrane utilized in this work has a hydraulic permeability of ~100 L m^{-2} h^{-1} bar^{-1}. The membrane with the P(AN-OEGMA-AHPMA) copolymer active layer coated on the PAN support has a permeability of ~1 L m^{-2} h^{-1} bar^{-1}. As a result, the resistance to flow provided by the support membrane relative to the copolymer active layer is negligible.[3]

3. Charge Functionalization and Inkjet Printing Protocol

Charged functional groups were introduced to the surface of the nanostructured membranes through the copper(I)-catalyzed azide-alkyne cycloaddition (CuAAC) "click" reaction mechanism. In particular, propargyl amine and propiolic acid were used to introduce positively-charged and negatively-charged functional groups, respectively. These alkynyl-terminated reactants (1.6 M), copper (II) sulfate pentahydrate ($CuSO_4 \cdot 5H_2O$) (120 mM), and ascorbic acid

(360 mM) were dissolved in a 4:1 (by weight) mixture of water and glycerol to generate the reactive ink solutions. Concentrated hydrochloride acid (HCl) was added until the pH of the reactive ink solutions was equal to pH ~1. This addition prevented the precipitation of copper. The two solutions were loaded into separate ink cartridges that were then inserted into an inkjet printer (Stylus C88+, Epson). The parent membrane was attached to a plastic sheet and sent through the printer, which was used to precisely control the deposition of the reactive solutions. After the deposition of the inks was complete, the reactants were allowed 10 minutes to diffuse into the pores and to react with the azido moieties. Subsequently, the membrane was removed from the plastic sheet and soaked in DI water to remove residual reactants. Single charge-functionalized membranes were generated by soaking the parent membranes in either the propiolic acid or propargyl amine reactive ink solution for 30 min. The membrane was rinsed and stored in DI water after the reaction.

4. Fourier Transform Infrared Spectroscopy

Membranes functionalized using the CuAAC reaction were analyzed using Fourier transform infrared spectroscopy (FTIR, Bruker Tenor 27). The membranes were rinsed using DI water and dried in a vacuum oven at room temperature for 12 hours to prepare them for analysis. Each sample was scanned 64 times over the range of wavenumbers from 400 to 4000 cm^{-1}. Full spectra of a parent membrane, a propiolic acid functionalized membrane and a propargyl amine functionalized membrane are displayed in Figure S7.

5. Fluorescent Microscopy

The fluorescent dyes rhodamine 6G and sulfo-cyanine5 alkyne (Lumiprobe) were dissolved in DI water at a concentration of 50 μM to prepare two fluorescent ink solutions. The ink solutions were used to print striped, cubic, and hexagonal patterns on a polysulfone

ultrafiltration membrane (Nanostone Water, Inc) as well as the parent copolymer membranes. After printing, the patterns were imaged using a fluorescence microscope (EVOS FL Auto, Thermo Fisher Scientific) equipped with RFP and Cy5 light cubes.

6. Scanning Electron Microscopy Energy Dispersive X-Ray Spectrscopy Analysis

A Magellen 400 Scanning Electron Microscope (SEM) combined with a Bruker Energy Dispersive X-Ray Spectrometer (EDX) was used for analyzing the progression of the CuAAC click reaction into the membrane. Membranes were functionalized using the same CuAAC reactions detailed in the main text, but in this case, 1.6 M propargyl chloride was used in place of the propargyl amine or the propiolic acid. This choice was made because the chlorine atom of propargyl chloride results in a distinct signal within the EDX spectrum that is easily detected relative to the signal from the copolymer. As such, elemental analysis of chlorine could be used to examine that the depth the functionalization reaction penetrated across the membrane. The 1.6 M propargyl chloride reactive solution was deposited on the surface of a P(AN-OEGMA-AHPMA) parent membrane and kept there for 1 hr, which is equivalent to the time needed to print a full membrane, before rinsing with DI water. The membrane was submerged in liquid nitrogen for 15 seconds and then fractured using tweezers to obtain an undisturbed cross section. SEM-EDX images and elemental maps were obtained using a current of 0.8 nA and an accelerating voltage of 15 kV.

7. Solute Transport Experiments

Solute rejection experiments were executed using an Amicon 8003 stirred cell (Millipore). A membrane was mounted in the base of the cell, which was then filled with a feed solution. The pH of the feed solution during the transport experiments was unadjusted and fell between a value of pH 5.5 to pH 6.0. The cell was connected to a source of compressed air, which drove the flow

of solution through the membrane at an applied pressure of 50 psi. The feed solution was stirred at a constant rate of 400 rpm to mitigate the effects of concentration polarization during all transport experiments. For each membrane examined, one to three permeate samples were collected in scintillation vials and stored until further analysis. The system was flushed with ~0.5 ml of DI water when switching between solutions containing different solutes.

8. Salt Transport Experiments

Four salts, potassium chloride (KCl), magnesium chloride ($MgCl_2$), potassium sulfate (K_2SO_4) and magnesium sulfate ($MgSO_4$), were investigated. For single solute transport experiments, the salt was dissolved in DI water at a concentration of 100 μM. For mixed solutes transport experiments, the membrane was challenged with a feed solution containing equimolar concentrations of KCl and $MgCl_2$ at four ionic strengths, 100 μM, 200 μM, 300 μM and 400 μM. The concentrations of K^+ and Mg^{2+} were measured using inductively coupled plasma optical emission spectroscopy (ICP-OES) (PerkinElmer Optima 8000) to infer the concentrations of potassium chloride and magnesium chloride. The concentration of SO_4^{2-} was measured using ion chromatography (IC) (Dionex ICS-5000) to infer the concentrations of potassium sulfate and magnesium sulfate. Given the concentrations of ions in the permeate and feed solutions, the percent rejection can be calculated as

$$Rejection\ (\%) = \left(1 - \frac{C_p}{C_f}\right) \times 100 \tag{S1}$$

where C_p represents the concentration of the ion in the permeate solution and C_f represents the concentration of the ion in the feed solution. In mixed salt experiments, the selectivity of the membrane for the permeation of K^+ over Mg^{2+} was according to Equation S2

$$Selectivity\ (K^+/Mg^{2+}) = \left(\frac{1 - R_{K^+}}{1 - R_{Mg^{2+}}}\right) \tag{S2}$$

where R_{K^+} and $R_{Mg^{2+}}$ are the observed rejection of K^+ and Mg^{2+}, respectively.

9. Neutral Solute Transport Experiments

For neutral solute transport experiments, the membranes were challenged with a feed solution containing either sucrose or poly(ethylene oxide) (PEO) dissolved in DI water at a concentration of 1 g L^{-1}. PEO molecules with molecular weights of 1.1, 4.0, and 6.0 kg mol^{-1} (all samples had a dispersity less than 1.1) were purchased from Polymer Source Inc. (Montreal, QC). Three permeate samples were collected for each test solution. The concentration of sucrose and PEO in these solutions was measured with a Shimadzu TOC-TN Organic Carbon Analyzer. Percent rejection was calculated using Equation S1.

10. Solving the Nernst-Planck and Poisson Equations in COMSOL

The steady-state variations in electrostatic potential and ion concentration near the surfaces of the charge-patterned membranes were examined using COMSOL Multiphysics. Specifically, by coupling the Electrostatics module with the Transport of Diluted Species module, COMSOL was used to simultaneously solve the Nernst-Planck equation for each ion (Equation S3) as well as the Poisson equation (Equation S4).

$$\nabla \cdot \left(-D_i \nabla c_i - z_i u_{m,i} \mathcal{F} c_i \nabla \phi\right) = 0 \quad \text{(S3)}$$

$$-\varepsilon \nabla^2 \phi = \rho_E \quad \text{(S4)}$$

The Nernst-Planck equation is written for both the cation and anion of a salt. The identity of the dissolved ion is represented by the subscript i with 1 indicating the cation and 2 representing the anion. D_i, c_i, z_i, and $u_{m,i}$ represent the diffusion coefficient, concentration, valence, and ionic mobility of species i, respectively. $\mathcal{F}$ is the Faraday constant. Note the convective terms are not included because the characteristic time for solution to permeate through the membrane is much greater than the characteristic time for the electrical double layer to develop near a charged surface. Specifically, for a dilute salt solution, the electrical double layer is formed in ~1 μs while it takes ~5 s for a characteristic volume of solution to permeate through the membranes. The Poisson

equation links the electrostatic potential, ϕ, to the local charge density, ρ_E. ε is the electrical permittivity of the salt solution, which was assumed equal to that of water. The value of ε is obtained by multiplying the relative permittivity of water (78.5) by the permittivity of free space.

11. Construction of the Patterned Membrane Control Volume and Boundary Conditions

The control volume for each system was established by drawing a simulation box with the charge-patterned membrane at the base, $x_3 = 0$. Unit cells consisted of stripes, cubes, and hexagons with a characteristic feature size between 100 nm and 5 μm. After executing the first series of simulations, it was identified that the interactions between the oppositely-charged domains were confined within a few Debye lengths (~100 nm) from the interfacial junctions. Therefore, feature sizes above 5 μm were not considered due to the unnecessary computational expense of the larger control volume. Because the characteristic time for permeation through the membrane was much longer than the time needed to establish the steady-state electrical double layer, the membrane was modeled as an impermeable plane with the total flux of ions through the plane at $x_3 = 0$ set to zero. The electrostatic potential at the membrane surface was determined by specifying the surface charge density of the domains. In particular, based on experimentally-determined values from a previous paper, the surface charge densities were set at values of 50 μC m^{-2} or -50 μC m^{-2}.

The volume on top of the membrane was filled with an aqueous solution containing dissolved ionic species (*i.e.*, K^+, Cl^-, Mg^{2+}, SO_4^{2-}). The identity of the ions was specified by assigning the values of the valence number and the diffusion coefficients. Assuming that the variation brought about due to the charge-patterned surface fully decay over the height of the simulation box, the solute concentration at the top of the box (x_3 = 200 nm) was set to the concentration of the bulk solution, 100 μM, and the electric potential was set to zero. Multiple simulation box heights were examined until this constraint was satisfied. Periodic boundary

conditions were utilized on all sides of the simulation box for the electric potential and the ion concentration.

12. Interfacial Packing Density Calculations for the Charge-Patterned Mosaic Membranes

Stripe-patterned (ST-CMM) and cubically-patterned (CU-CMM) membranes

Assume a unit of membrane in the shape of a square with an area of L^2. In this square, the oppositely charged domains are represented by blue and red stripes (Figure S9). The width of each stripe has a constant value of D. In Figure S9, the interfacial region between the oppositely charged domains is highlighted by yellow lines. For a ST-CMM, all of the lines align parallel to the d_1 axis. The total length of interfacial regions can be calculated by multiplying the length of the line (L) by the number of lines within the membrane area. The number of lines in a given unit is equal to

$$n_{d2} = \frac{L}{D} - 1 \tag{S5}$$

Because the membranes are fabricated on the centimeter scale with stripe widths on the micrometer scale, $\frac{L}{D} \gg 1$, and the number of lines can be approximated as $\frac{L}{D}$. Hence, the total length of the interfacial regions for a ST-CMM is

$$L_{ST} = \frac{L^2}{D} \tag{S6}$$

The interfacial packing density is derived by normalizing the total length of interfacial regions using the membrane area,

$$\sigma_{ST} = \frac{L^2/D}{L^2} = \frac{1}{D} \tag{S7}$$

The derivation of the interfacial packing density for a CU-CMM is similar to that for the ST-CMM except the interfacial regions along both the d_1 and d_2 axes (Figure S9B and S9C, respectively) must be accounted for. Hence, the total length of interfacial region for a CU-CMM is

$$L_{CU} = \frac{L^2}{D} + \frac{L^2}{D} = \frac{2L^2}{D} \tag{S8}$$

Giving an interfacial packing density of

$$\sigma_{CU} = \frac{2L^2/D}{L^2} = \frac{2}{D} \tag{S9}$$

for a CU-CMM.

Hexagonally-patterned (HE-CMM) membranes

A membrane unit in the shape of a parallelogram with a base length of L is assumed to derive the interfacial packing density for a HE-CMM. The parallelogram has an area of $\frac{\sqrt{3}}{2}L^2$. Within the parallelogram, the triangles that make up the hexagonal pattern have a characteristic feature size given by their height, D. The oppositely charged domains share boundaries in three principal directions, d_1, d_2, and d_3. Hence, the total length of the interfacial regions can be divided into three directions and calculated separately.

In all directions, the length of the borders is equal to the number of borders multiplied by the length of each border. In the d_1 and d_2 directions, this is given by the following expression

$$L_{d1} = L_{d2} = \left(\frac{\sqrt{3}L}{2D} - 1\right) \times L \cong \frac{\sqrt{3}L^2}{2D} \tag{S10}$$

where the fact that the feature size is smaller than the membrane size has been used to simplify the expression.

In the d_3 direction (Figure S9F), the borders between the oppositely charged domains are of different lengths. However, by recognizing that the shortest border can be combined with the second longest border to give a line of line L, and that the second shortest border can be combined with the third longest border to give the same, and so on, until $\frac{\sqrt{3}L}{2D}$ borders of length L are identified, the total length of borders in d_3 direction is found to be

$$L_{d3} = \frac{\sqrt{3}L^2}{2D} \tag{S11}$$

Thus, the total length of the borders for the HE-CMM membrane is

$$L_{HE} = L_{d1} + L_{d2} + L_{d3} = \frac{3\sqrt{3}L^2}{2D} \tag{S12}$$

By normalizing the total length of borders using the membrane area $\frac{\sqrt{3}}{2}L^2$, the following expression for the packing density of a hexagonally patterned membrane can be obtained.

$$\sigma_{HE} = \frac{\frac{3\sqrt{3}L^2}{2D}}{\frac{\sqrt{3}}{2}L^2} = \frac{3}{D} \tag{S13}$$

13. Derivation of Total Salt Flux through the Charge-Patterned Mosaic Membranes

The salt flux, J_s, can be calculated based on the following equation

$$Rejection(\%) = \left(1 - \frac{C_p}{C_f}\right) \times 100 = \left(1 - \frac{J_s \cdot \rho_w}{J_w C_f}\right) \times 100 \tag{S14}$$

where J_s and J_w are the salt flux and the water flux through the membrane, respectively; C_f is the salt concentration in the feed solution; and ρ_w is the density of water. By rearranging the equation,

$$J_s = \left(1 - \frac{R(\%)}{100}\right) \cdot \frac{C_f}{\rho_w} \cdot J_w \tag{S15}$$

The values calculated for J_s are plotted in Figure S11.

Supporting Figures

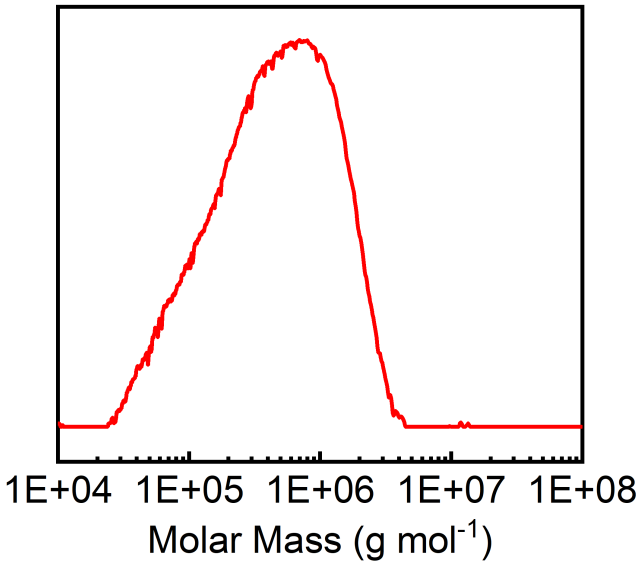

Figure S1. GPC trace of the P(AN-OEGMA-AHPMA) copolymer.

Gel permeation chromatography (GPC) trace of the P(AN-OEGMA-AHPMA) copolymer using DMF as the eluent at a flow rate of 1 mL min^{-1}. The GPC was calibrated using polymethyl methacrylate standards. The trace indicates a number average molar mass of 191 kg mol^{-1} and a dispersity ($Đ$) value of 3.0.

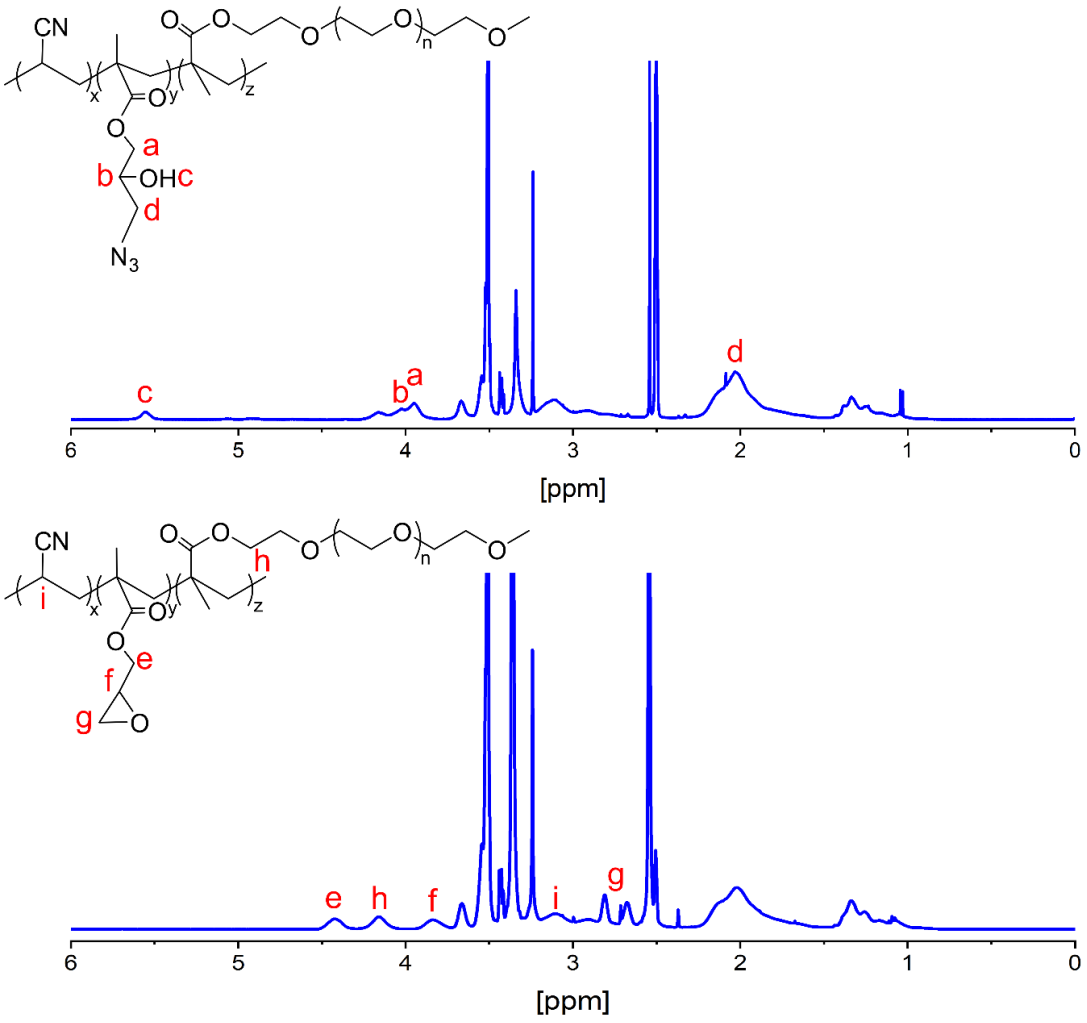

Figure S2. ^{1}H NMR spectra of the P(AN-OEGMA-AHPMA) copolymer.

^{1}H NMR spectra of the poly[acrylonitrile-*co*-oligo(ethylene glycol) methyl ether methacrylate-*co*-(3-azido-2-hydroxypropyl methacrylate)] [P(AN-OEGMA-AHPMA)] copolymer (top) and the poly[acrylonitrile-*co*-oligo(ethylene glycol) methyl ether methacrylate-*co*-(glycidyl methacrylate)] [P(AN-OEGMA-GMA)] copolymer (bottom). The disappearance of characteristic double peaks **g** associated with the protons of the epoxide moiety and the appearance of peak **c**, which is associated with the hydroxyl group, indicated the success of the ring opening reaction. Integration of the peaks **e**, **h**, and **i** was used to determine the relative compositions of the GMA, OEGMA, and AN repeat units within the copolymer, respectively.

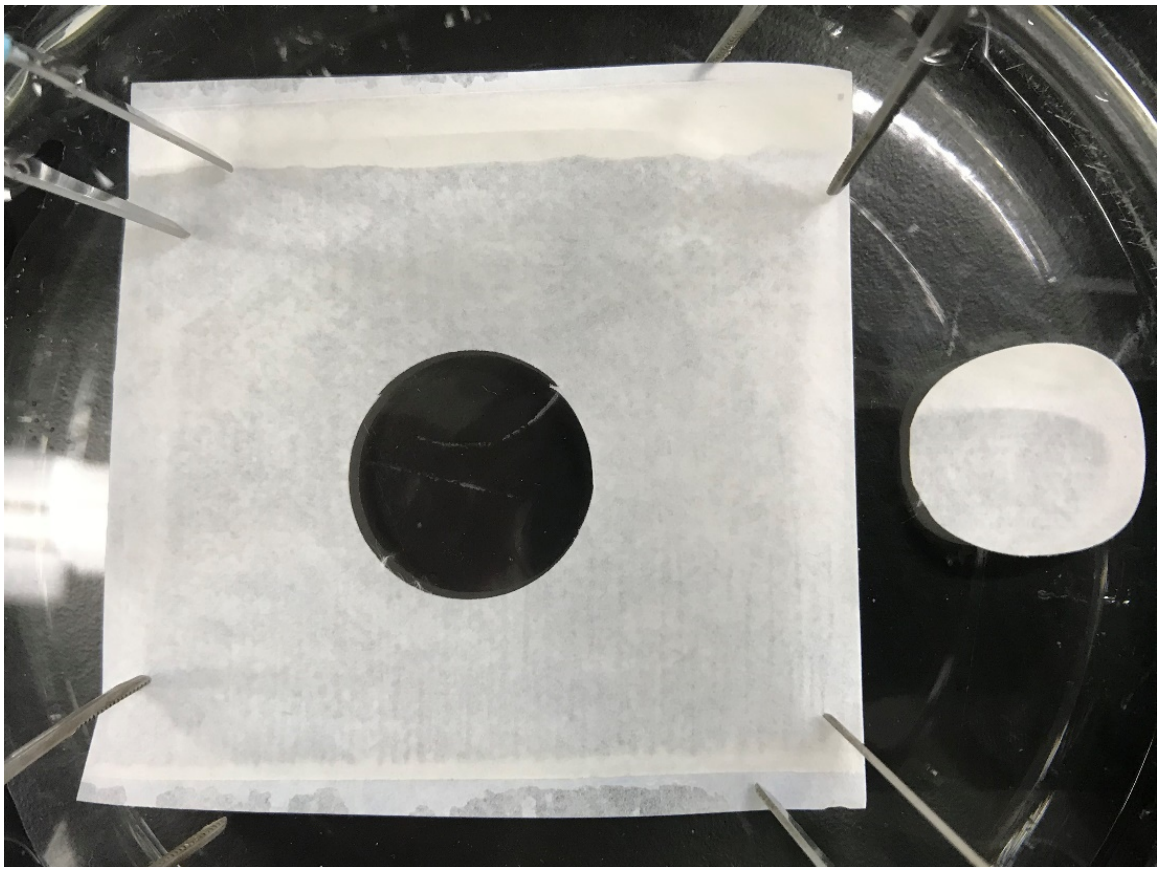

Figure S3. An image of the as-cast membrane.

A picture of an as-cast P(AN-OEGMA-AHPMA) parent membrane. The membrane was cast from a solution containing 20% (by weight) P(AN-OEGMA-AHPMA) copolymer dissolved in dimethyl sulfoxide (DMSO). The solution was cast onto a PX PAN ultrafiltration membrane using a doctor's blade a set at a gate height of 38 μm. After being drawn into a film, solvent was allowed to evaporate for 5 min before plunging the film into an isopropyl alcohol bath. The membrane remained in the nonsolvent bath for at least two hours to ensure full solvent exchange. It was then transferred to and stored in DI water.

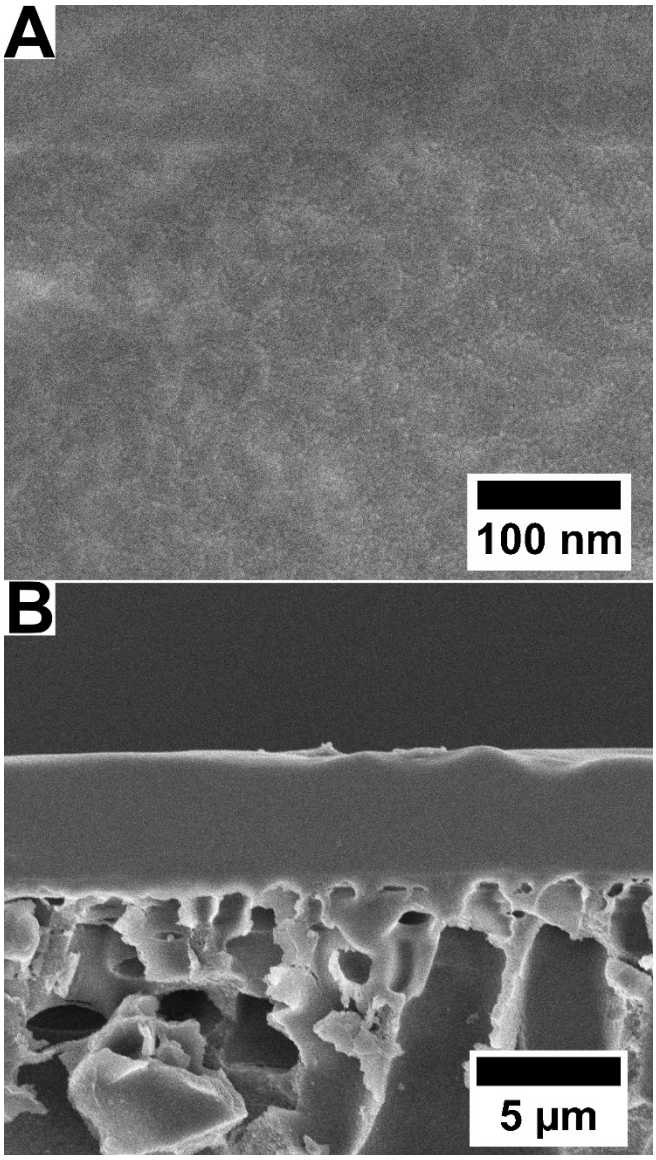

Figure S4. SEM micrographs of the parent copolymer membrane.

Scanning electron microscopy (SEM) micrographs of a P(AN-OEGMA-AHPMA) copolymer membrane: (**A**) a top-down surface view and (**B**) a cross-sectional view. The top surface micrograph demonstrates a defect-free surface consistent with the pore size of ~5 nm estimated from solute rejection tests. While the 5 nm pores are too small to observe using SEM, the values estimated from solute rejection are corroborated by high-resolution TEM micrographs and SAXS data reported in other studies on this family of copolymer materials.[4,5] The cross-sectional view displays an active layer thickness of ~ 5 µm.

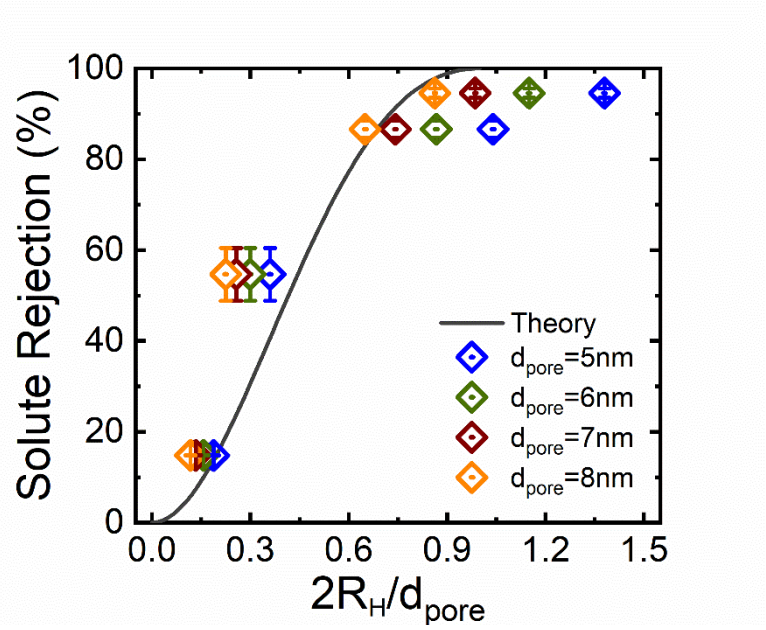

Figure S5. Neutral solute rejection by the parent copolymer membrane.

Solute rejection curve for the azide parent membranes. Neutral molecules, *i.e.,* sucrose (342 g mol^{-1}) and poly(ethylene oxide) (PEO) samples with molecular weights of 1.1, 4.0, and 6.0 kg mol^{-1} were dissolved in DI water to generate the four feed solutions. The concentrations of these solutes in the feed and permeate solutions were quantified using total organic carbon analysis. The hydrodynamic radii of the molecules, R_H, were determined from the value of their diffusion coefficient in water. The hindered transport theory based on work from Zeman and Wales was plotted to fit the expermental results.[6] Diameters varying from 5 nm to 8 nm were compared with the theory to estimate the pore size.

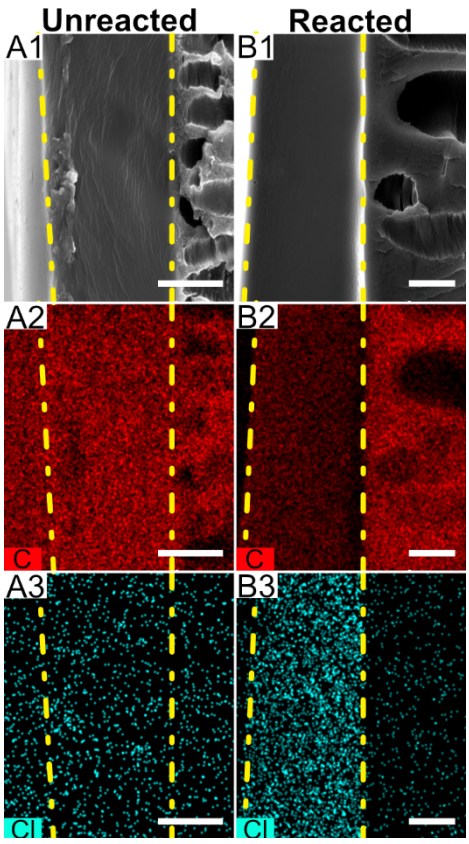

Figure S6. SEM-EDX analysis of parent and functionalized copolymer membranes.

(**A1**, **B1**) Cross-sectional view SEM micrographs of the (**A1**) unreacted and (**B1**) propargyl chloride reacted copolymer membranes. The membranes were prepared using the same experimental conditions as the charge-patterned membranes. However, the charge-functionalized alkyne-terminated reactants were replaced with propargyl chloride. To guide the reader's eye, the copolymer active layer is indicated by the region between the two, yellow dashed. (**A2**, **B2**) Energy-dispersive x-ray spectroscopy (EDX) elemental maps of carbon for the (**A2**) unreacted copolymer membrane and (**B2**) reacted copolymer membrane. (**A3**, **B3**) EDX elemental map for chlorine for the (**A3**) unreacted copolymer membrane and (**B3**) propargyl chloride reacted membrane. The chlorine-rich regions, indicated in cyan, in combination with the FTIR spectra for these membranes indicate the covalent attachment of the alkyne-terminated reactant over the whole membrane cross section. Scale bar represents 5 μm.

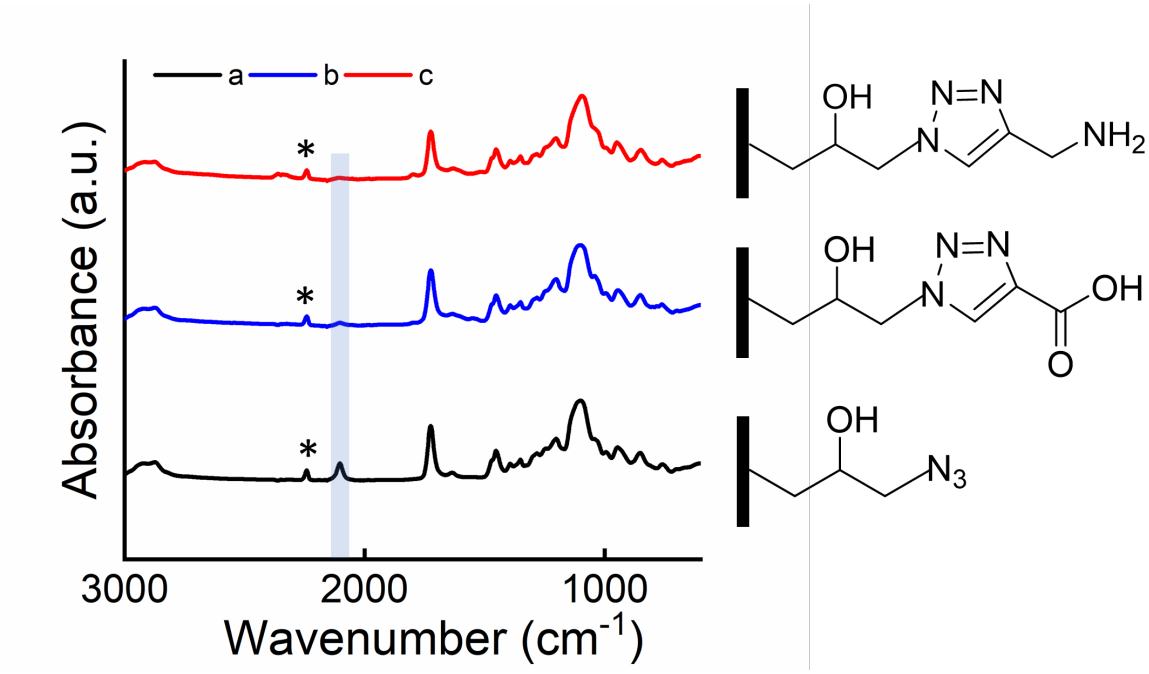

Figure S7. FTIR spectra of the charge-functionalized membranes.

Full FTIR spectra of **a.** an azide parent membrane **b.** an acid-functionalized membrane generated by printing 5 overprints of a reactive propiolic acid solution at a resolution of 720 dots per inch (DPI) **c.** an amine-functionalized membrane printed using 5 overprints of a propargyl amine reactive ink solution at a resolution of 720 DPI.

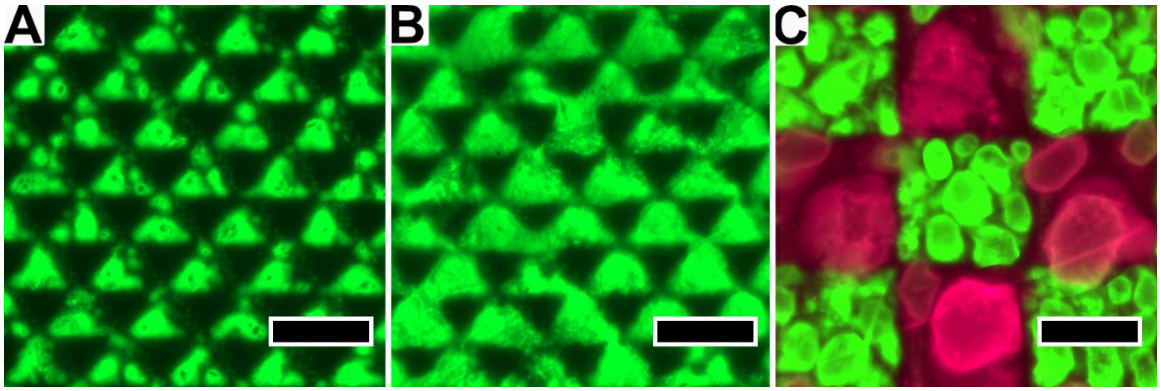

Figure S8. Fluorescent micrographs of charge-functionalized membranes.

Fluorescent micrographs of copolymer membranes with. All patterns were printed using a resolution of 720 DPI; the number of overprints was changed. (**A**) A hexagonally-patterned surface printed using 1 overprint of a single functional ink solution. (**B**) A hexagonally-patterned surface printed using 5 overprints of a single functional ink solution. (**C**) A cubically-patterned surface printed using 5 overprints of two functional ink solutions. The ink solutions were prepared by dissolving rhodamine 6G (60 μM) and sulfo-cyanine5 azide at a concentration of ~100 μM in DI water, respectively. A fluorescent microscope equipped with RFP and Cy5 light cubes was used to visualize patterned surface. The domains containing Rhodamine 6G appear green and the domains containing sulfo-cyanine5 alkyne appear pink. The scale bars represent 500 μm.

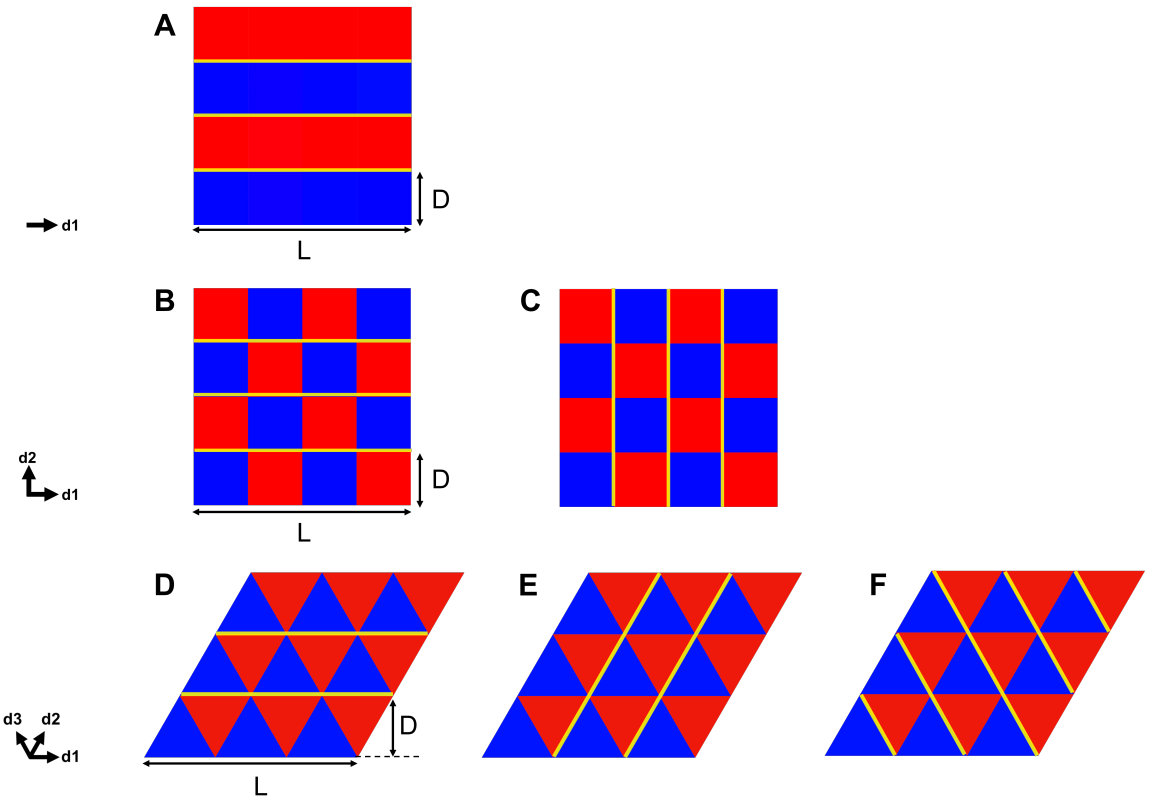

Figure S9. Schematics of used to calculate interfacial packing density.

Schematics of the (**A**) stripe-patterned and (**B-C**)**.** cubically-patterned membranes. The interfacial regions between the oppositely charged domains, which are highlighted by the yellow lines, are grouped into two directions, d_1 and d_2. The membrane unit is a square with sides of length L and characteristic feature sizes D. Schematics of the (**D-F**) hexagonally patterned membranes. The interfacial regions between the oppositely charged domains are grouped into three directions, d_1, d_2, and d_3. The membrane unit is a parallelogram with a base length, L. The characteristic feature size of the pattern is the height of the equilateral triangles, D.

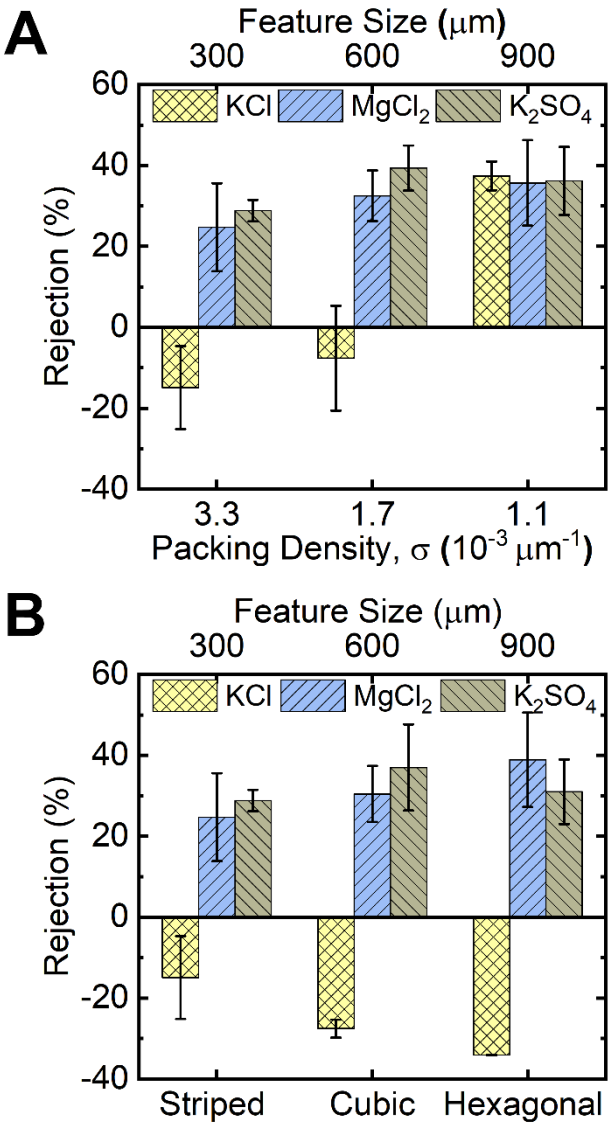

Figure S10. Salt rejection of CMMs with fixed geometry and constant σ.

Comparing the results of the single salt rejection experiments in a different manner reinforces that it is the variation in σ, and not another geometric consideration, that is influencing ion permeation. (**A**) Single salt rejection values of stripe-patterned mosaic membranes with varied feature sizes and values of interfacial packing density isolates the effect of the interfacial packing density for the ST-CMM pattern geometry. For ST-CMMs with D from 900 μm to 300 μm, the transport of KCl transitions from rejection to enrichment as D decreases and σ increases. (**B**) Single salt rejection values of charge-patterned membranes with interfacial packing density value of ~3.3×10^{-3} μm^{-1} isolates the effect of pattern geometry for constant values of σ. For three membranes with highly variable patterns and feature sizes but a consistent value of σ at 3.3×10^{-3} μm^{-1} (*i.e.*, a D = 300 μm ST-CMM, a D = 600 μm CU-CMM, and a D = 900 μm HE-CMM), the enrichment of KCl was nearly constant, which indicates that pattern geometry alone did not have a significant impact. Error bars represent one standard deviation, which was calculated based on 4 permeate samples collected from two membranes of the same type.

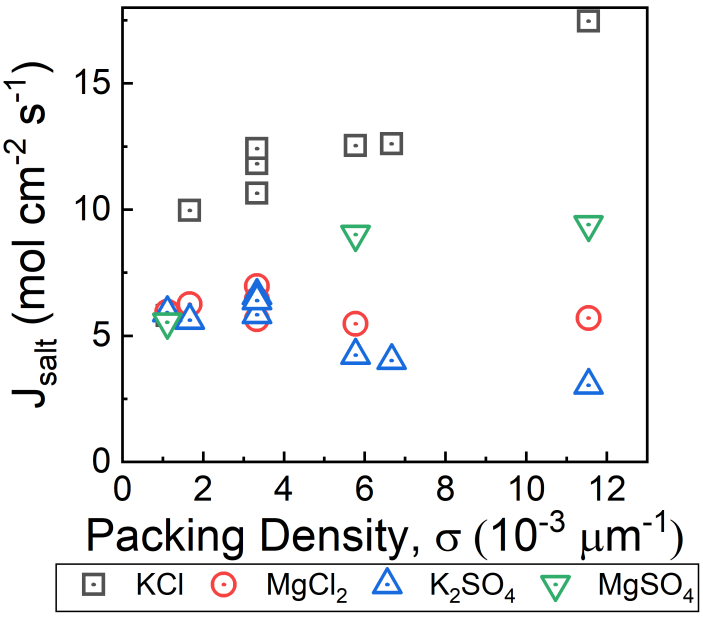

Figure S11. Salt flux across the CMMs with varying interfacial packing density.

The salt flux was calculated using the values of the percent rejection reported in Figure 3 in conjunction with Equation S15 and the values of the water flux measured during rejection experiments.

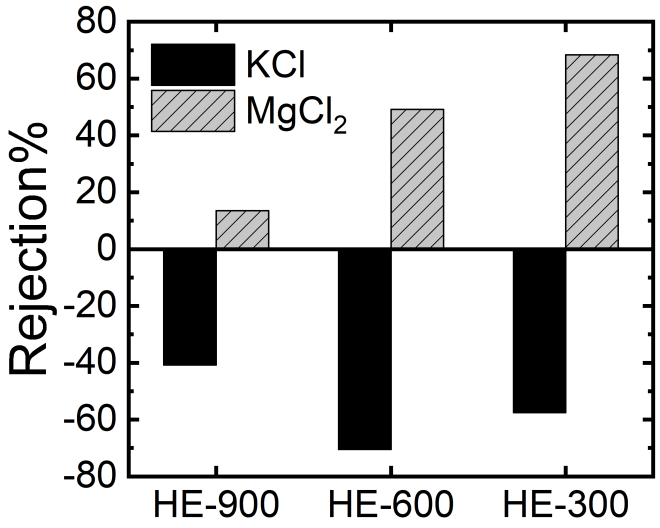

Figure S12. Results of mixed salt rejection.

Solute rejection of KCl and $MgCl_2$ from a mixture of two salts with total ionic strength of 200 μM. Hexagonally patterned mosaic membranes with feature size of 300 μm, 600 μm and 900 μm were used. The enrichment of K^+ and rejection of Mg^{2+} was consistent with results obtained from single solute rejection experiments.

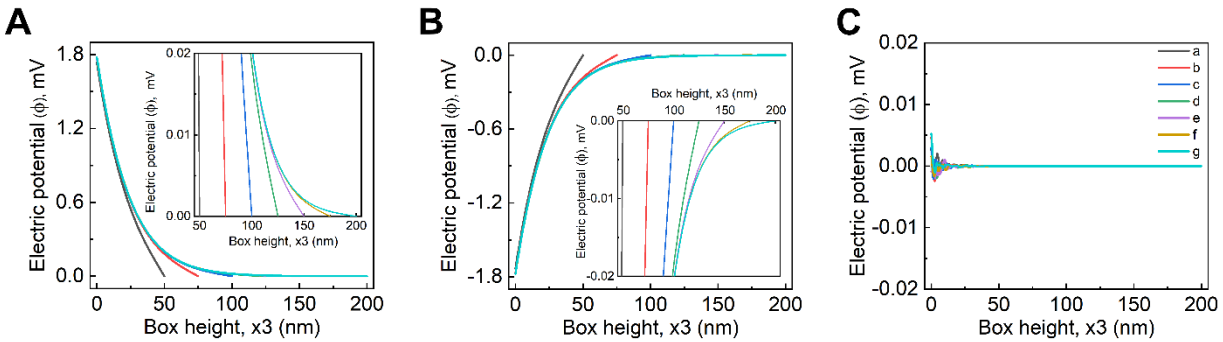

Figure S13. Variation of the electric potential in the x_3-direction.

The variation in the electric potential from the membrane surface to the top of the simulation box, (**A**) at the midpoint of the positively-charged domain. (**B**) at the midpoint of the negatively-charged domain, and (**C**). at the interface between the cationic and anionic domains. Simulation box heights from 50 nm to 200 nm, in 25 nm increments, are represented by the curves labeled **a** to **g**, respectively. In all cases, the electric potential at the membrane surface was determined by the fixed surface charge density boundary condition. As the distance from the membrane increases, *i.e.*, as the value of x_3 increases, the electric potential decays toward a reference value of 0 indicative of the electroneutral bulk solution. Since the boundary condition, at the top of the simulation box is meant to approximate the behavior as x_3 tends to infinity, the solution for the electrical potential should be independent of the box height. The variations in electrostatic potential were independent of the box height for simulations with a box height, $x_3 \geq 200$ nm). Note: the value of the electric potential at the interface between the charged domains plotted in panel (**C**) is an order of magnitude smaller than that in panels (**A**) and (**B**).

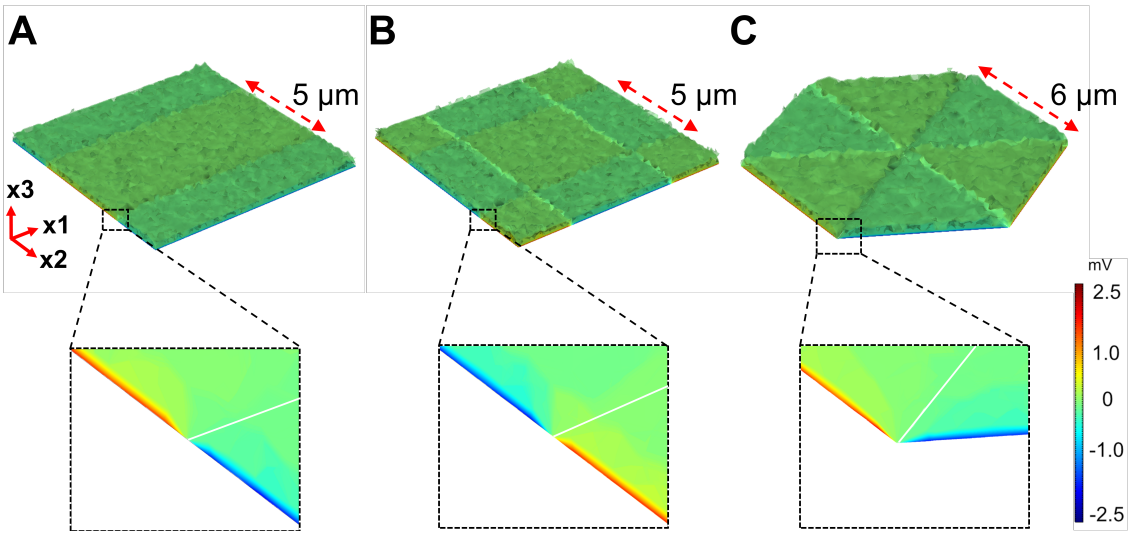

Figure S14. Spatial variation of the electric potential over the membrane surface.

(**A-C**) Local variation in the electric potential distribution for membranes of 5 µm feature size. Each system consisted of a unit cell of the patterned membrane at bottom and a volume of solution above the membrane-solution interface. The cell was filled with a salt solution at a concentration of 100 µM. The results shown are representative of a 1:1 salt such as KCl. The surface charge density of the membrane was set to 50 µC m^{-2} and -50 µC m^{-2} for the positive and negative domains, respectively. Each charge-functionalized domain has a feature size of 5 µm. The simulation box height was set to 10 µm.

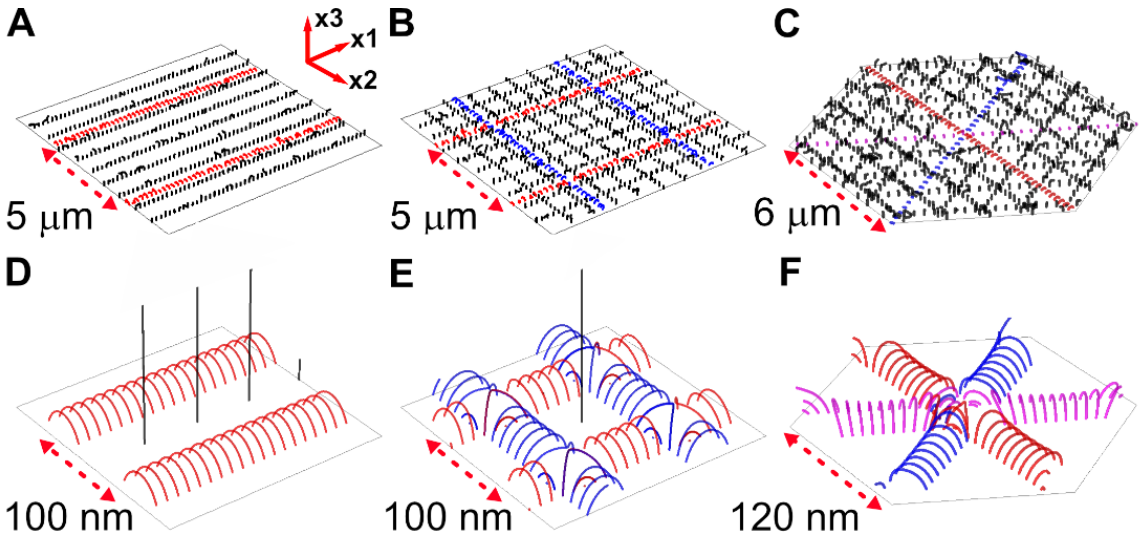

Figure S15. Spatial variation of the electrical field lines near interfacial junctions.

Three-dimensional plot of electrical field lines near the interfacial regions between oppositely charged domains. The electrical field lines were colored along different orientations as red, blue and magenta lines represent the "membrane-to-membrane" communication and the black lines represent the "membrane-to-solution" communication. Mosaic units of feature size 5 μm (**A-C**) and 100 nm (**D-F**) were compared. **A-F**. angled view of a ST-CMM unit (**A, D**), a CU-unit (**B, E**) and a HE-CMM unit (**C, F**). The side length of the HE-CMM was set to be 6 μm and 120 nm so that the feature size of the pattern was close to 5 μm and 100 nm. In ST-CMM, the oppositely charged domains communicate in a single orientation; in CU-CMM, the oppositely charged domains communicate in two orientations; in HE-CMM, the oppositely charged domains communicate in three orientations. The simulation box height was set to be 10 μm in A, B and C and 200 nm in D, E and F.

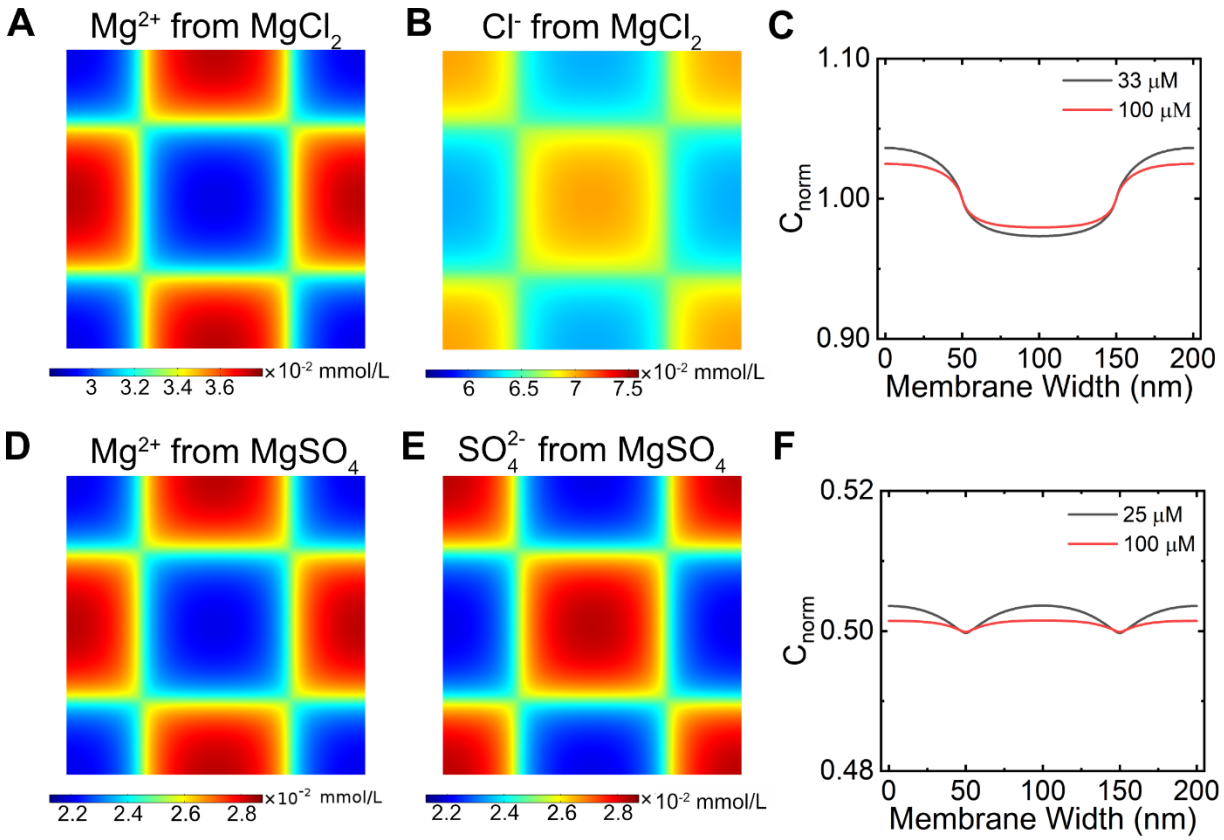

Figure S16. Distribution of ions from $MgCl_2$ and $MgSO_4$ at varying concentrations.

Top-down view of concentration distribution of ions from dissolved $MgCl_2$ (**A, B**) and $MgSO_4$ (**D, E**) with the concentration of 33 μM and 25 μM, respectively. The ionic strength of both solutions was 100 μM. (**A**) Mg^{2+} (**B**) Cl^- (**D**) Mg^{2+} (**E**) SO_4^{2-}. Stoichiometry-normalized concentration of the salt at two solution concentrations: 33 μM and 100 μM for $MgCl_2$ (**C**); 25 μM and 100 μM for $MgSO_4$ (**F**) was plotted. The values of the stoichiometry-normalized salt concentration presented were obtained from a horizontal line drawn through the midline of the membrane unit. The system consisted of a cubically patterned mosaic surface with a feature size of 100 nm. The square at the center of the pattern was positively charged.

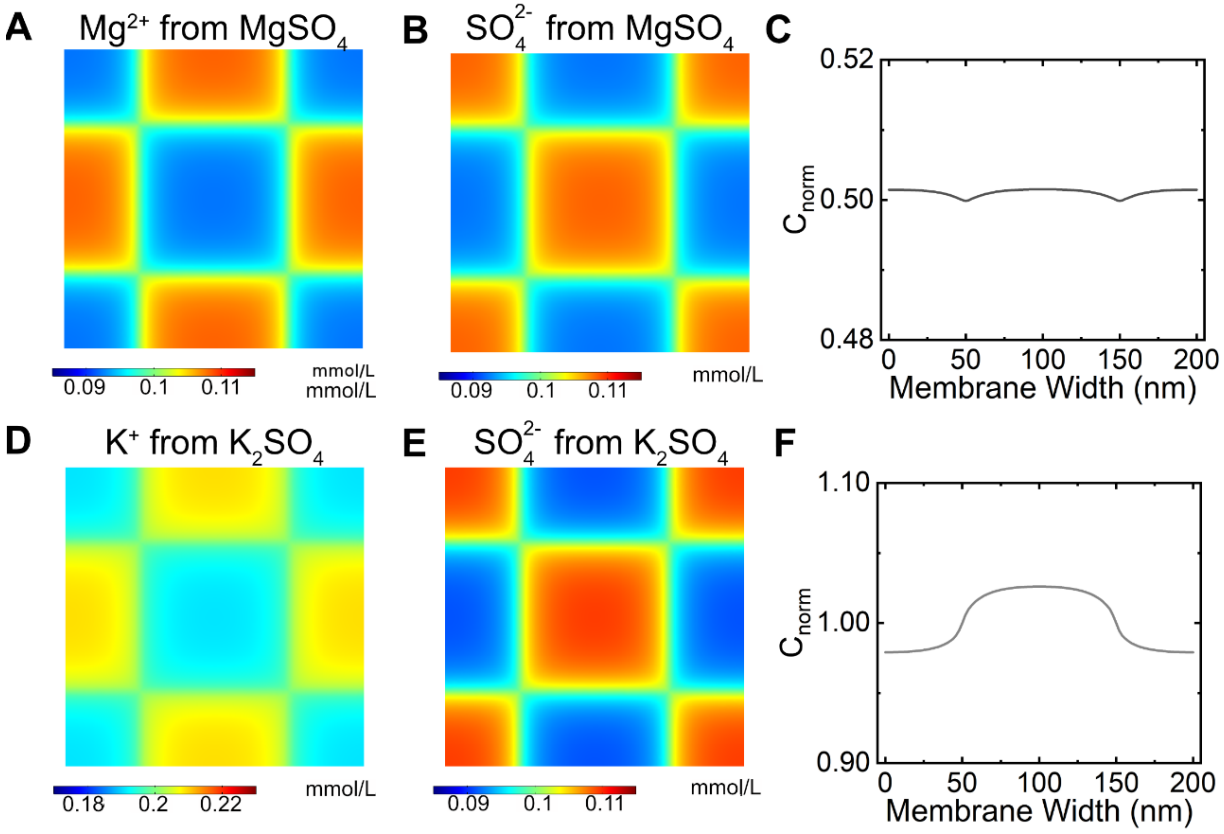

Figure S17. Distribution of ions from $MgSO_4$ and K_2SO_4.

Top-down view of concentration distribution of ions from dissolved $MgSO_4$ (**A, B**) and K_2SO_4 (**D, E**). (**A**) Mg^{2+} (**B**) SO_4^{2-} (**D**) K^+ (**E**) SO_4^{2-}. Stoichiometry-normalized concentration of the salt, defined by Equation 2, was plotted for $MgSO_4$ (**C**) and K_2SO_4 (**F**). The values of the stoichiometry-normalized salt concentration presented were obtained from a horizontal line drawn through the midline of the membrane unit. The system consisted of a cubically patterned mosaic surface with a feature size of 100 nm and a solute concentration of 100 μM. The square at the center of the pattern was positively charged.

References

1. Qu, S.; Dilenschneider, T.; Phillip, W. A. Preparation of Chemically-Tailored Copolymer Membranes with Tunable Ion Transport Properties. *ACS Appl. Mater. Interfaces* **2015**, *7*, 19746–19754.
2. Qu, S.; Shi, Y.; Benavides, S.; Hunter, A.; Gao, H.; Phillip, W. A. Copolymer Nanofilters with Charge-Patterned Domains for Enhanced Electrolyte Transport. *Chem. Mater.* **2017**, *29*, 762–772.
3. Zhang, Y.; Mulvenna, R. A.; Boudouris, W.; Phillip, W. A. Nanomanufacturing of High-Performance Hollow Fiber Nanofiltration Membranes by Coating Uniform Block Polymer Films from Solution. *J. Mater. Chem. A,* **2017**, *5*, 3358–3370.
4. Rathee, V. S.; Qu, S.; Phillip, W. A.; Whitmer, J. K. A Coarse-Grained Thermodynamic Model for the Predictive Engineering of Valence-Selective Membranes. *Mol. Syst. Des. Eng.* **2016**, *1*, 301–312.
5. Bush, A. M.; Ford, H. O.; Gao, F.; Summe, M. J.; Rouvimov, S.; Schaefer, J. L.; Phillip, W. A.; Guo, R. Tunable Mesoporous Films from Copolymers with Degradable Side Chains as Membrane Precursors. *J. Memb. Sci.* **2018**, 567, 104–114.
6. Zeman, L.; Wales, M. In *Synthetic Membranes: Volume II*; American Chemical Society: Washington, DC, **1981**; 411–434.